IOP PUBLISHING PHYSICS IN MEDICINE AND BIOLOGY

Phys. Med. Biol. 56 (2011) 965–977 doi:10.1088/0031-9155/56/4/006

A feasibility study of a molecular-based patient setup verification method using a parallel-plane PET system

Satoshi Yamaguchi[1], Masayori Ishikawa[1], Gerard Bengua[2], Kenneth Sutherland[1], Teiji Nishio[3], Satoshi Tanabe[1], Naoki Miyamoto[1], Ryusuke Suzuki[2] and Hiroki Shirato[4]

[1] Department of Medical Physics and Engineering, Hokkaido University Graduate School of Medicine, N-15 W-7 Kita-ku Sapporo 060-8638, Japan
[2] Department of Medical Physics, Hokkaido University Hospital, N-14 W-5 Kita-ku Sapporo 060-8648, Japan
[3] Particle Therapy Division, Research Center for Innovative Oncology, National Cancer Center, Kashiwa, 6-5-1 Kashiwano-ha, Kashiwa-shi, Chiba 277-8577, Japan
[4] Department of Radiology, Hokkaido University Graduate School of Medicine, N-15 W-7 Kita-ku Sapporo, 060-8638 Japan

E-mail: masayori@med.hokudai.ac.jp

Received 15 July 2010, in final form 9 December 2010
Published 19 January 2011
Online at stacks.iop.org/PMB/56/965

Abstract

A feasibility study of a novel PET-based molecular image guided radiation therapy (m-IGRT) system was conducted by comparing PET-based digitally reconstructed planar image (PDRI) registration with radiographic registration. We selected a pair of opposing parallel-plane PET systems for the practical implementation of this system. Planar images along the in-plane and cross-plane directions were reconstructed from the parallel-plane PET data. The in-plane and cross-plane FWHM of the profile of 2 mm diameter sources was approximately 1.8 and 8.1 mm, respectively. Therefore, only the reconstructed in-plane image from the parallel-plane PET data was used in the PDRI registration. In the image registration, five different sizes of ^{18}F cylindrical sources (diameter: 8, 12, 16, 24, 32 mm) were used to determine setup errors. The data acquisition times were 1, 3 and 5 min. Image registration was performed by five observers to determine the setup errors from PDRI registration and radiographic registration. The majority of the mean registration errors obtained from the PDRI registration were not significantly different from those obtained from the radiographic registration. Acquisition time did not appear to result in significant differences in the mean registration error. The mean registration error for the PDRI registration was found to be 0.93 ± 0.33 mm. This is not statistically different from the radiographic registration which had a mean registration error of 0.92 ± 0.27 mm. Our results suggest

0031-9155/11/040965+13$33.00

that m-IGRT image registration using PET-based reconstructed planar images along the in-plane direction is feasible for clinical use if PDRI registration is performed at two orthogonal gantry angles.

(Some figures in this article are in colour only in the electronic version)

1. Introduction

Image guided radiotherapy (IGRT) techniques are presently used clinically to improve the accuracy of treatment delivery in photon radiation therapy. IGRT is used to correct for patient positioning errors prior to or during treatment by using image guided procedures. Patient setup can be verified through the co-registration of digitally reconstructed radiographs (DRR) and imaging plate (IP) or electronic portal imaging device (EPID) images taken using MV-x rays from a linear accelerator (Linac) while the patient is set up just prior to treatment (Dong and Boyer 1995, Gilhuijs *et al* 1996). Linac systems with on-board cone-beam computed tomography (CBCT) devices have also been developed (Pouliot *et al* 2005, Jaffray *et al* 2002, Groh *et al* 2002, Ford *et al* 2002, Munbodh *et al* 2006). CBCT allows the imaging of the target volume and organs at risk during treatment. Accuracy of patient setup verification error is important in order to ensure that the actual treatment geometry is as close as possible to the treatment planning geometry. At present, patient setup verification is done mostly by the alignment of bony structures in radiographic images taken during treatment and those used for treatment planning. The change in the tumor size and location inside the body is usually difficult to determine during treatment. Making the tumor visible in the irradiation field is thus desirable in order to improve setup verification accuracy.

Positron emission tomography (PET) based on sugar metabolism in the tumor caused by ^{18}F-fluorodeoxyglucose (FDG) uptake has been shown to be effective for distinguishing the tumor during diagnosis (Som *et al* 1980). Since PET images are functional images, they allow cell activity to be visible; thus, the tumor position can be determined. Another promising radioactive tracer for PET imaging is ^{18}F-fluoromisonidazole (FMISO) (Nehmeh *et al* 2008). FMISO is able to delineate hypoxic cells, which are known to be radiation resistant, in tumors. Clinical trials have demonstrated improved tumor control by delivering escalated doses to hypoxic tumor cells using IMRT and other techniques (Lee and Le 2008).

The spatial resolution and sensitivity of recent PET devices have also been significantly improved. This has been partly due to (1) the development of new detector elements such as BGO or GSO crystals, (2) the change in the acquisition method from 2D to 3D, and (3) the invention of depth-of-interaction (DOI) (Wienhard *et al* 2002, Yamaya *et al* 2003). The application of PET technology as a new modality for diagnostic procedures is also now being considered, for example, positron emission mammography (PEM) (Smith *et al* 2003, Huesman *et al* 2000, Zhang *et al* 2007, Raylman *et al* 2008, MacDonald *et al* 2009). In this study, we propose a PET-based molecular image guided radiation therapy (m-IGRT) system for patient setup verification in cases where significant tumor shrinkage or growth may occur, such as intracranial or head and neck. In the practical implementation of an m-IGRT system, it is preferable that the PET device is combined with a radiotherapy gantry to guarantee mechanical precision. There are, however, some restrictions on how the PET detectors can be mounted to the present gantry systems.

Because PET is a device that detects the annihilation radiation caused by positrons, it is necessary that at least a pair of opposed detectors are arranged to detect the two photons simultaneously. It is preferable that the isocenter of the pair of opposed detectors is identical to the isocenter of the radiotherapy unit. A structure with a wide open space between a pair of

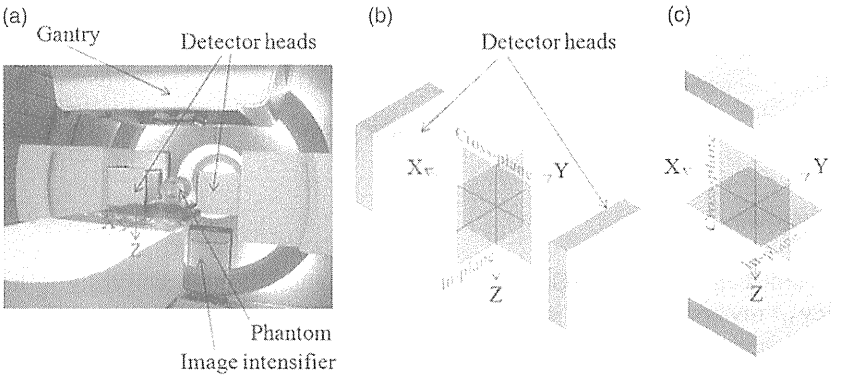

Figure 1. (a) The BOLPs with its gantry positioned at 0°. (b) The orientations of the in-plane and cross-plane directions in the BOLPs at a gantry angle of 0°. (c) The orientations of the in-plane and cross-plane directions in the BOLPs at a gantry angle of 90°.

opposed detectors is also needed so that the mega-voltage irradiation field does not become obstructed. The gantry rotation of the radiotherapy unit and the movement or the rotation of the couch must also be considered. Moreover, it is necessary to secure a wide field of view to use the device for setup verification. However, it is difficult in the conventional PET detector geometry, with ring-shape arrangement, to achieve this purpose. We therefore selected a geometry with a pair of opposing parallel-plane detectors. The advantage of this detector geometry is that it is structurally simple, and that it can be mounted easily on a radiotherapy gantry, similar to on-board imaging (OBI) devices.

In order to evaluate the feasibility of molecular image guided registration, we used the beam on-line PET system (BOLPs), developed at the Particle Therapy Division of the National Cancer Center, Kashiwa (Nishio *et al* 2005, 2006, 2010). The system consists of a pair of opposing parallel-plane detectors mounted on the gantry which can detect annihilation radiation produced by positron emitters (e.g. ^{15}O, ^{14}O, ^{13}N and ^{11}C). The BOLPs was originally developed for visualizing irradiation fields by measuring the activity of positron emitters which are generated by nuclear reactions from incident proton beams. The BOLPs has the same detector configuration as that of our proposed system.

In this paper, we report on the feasibility of a novel m-IGRT by comparing the PET-based digitally reconstructed planar image (PDRI) registration with radiographic registration.

2. Materials and method

2.1. Beam on-line PET system

The BOLPs at the National Cancer Center, Kashiwa, in Japan was used to verify the accuracy of patient setup verification in our proposed parallel-plane PET system. The BOLPs detector is mounted at the gantry of the proton irradiation system as shown in figure 1(a). The detector head consists of 3960 BGO crystals (2 mm × 2 mm × 20 mm) covering a 16 × 16 cm^2 field of view. The distance between the detector heads was fixed at 40 cm. Shown in figure 1(b) are the orientations of the in-plane and cross-plane directions for a gantry angle of 0°. The orientations of the in-plane and cross-plane directions for a gantry angle of 90° are illustrated in figure 1(c). The evaluation of the full width at half maximum (FWHM) of the profile of

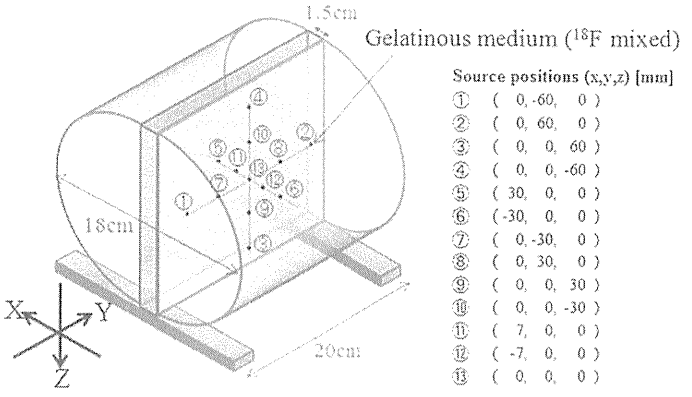

Figure 2. Cylindrical phantom with ^{18}F-sources placed in the positions as indicated.

2 mm diameter sources was done along the cross-plane and in-plane directions for a gantry angle of 0°. The FWHM of the profile is indicative of the spatial resolution.

In the image registration, only the reconstructed in-plane image from the parallel-plane PET data was used, and from here on, this in-plane image will be referred to as PDRI.

The BOLPs also includes an on-board x-ray system that allows the acquisition of radiographic images for patient setup verification. We compared the accuracy of radiographic and PDRI registrations.

2.2. Image reconstruction method

The detector configuration of the BOLPs is different from that of conventional PET systems in that they do not encircle the subject. Due to the parallel placement of the detector heads, there is limited angular sampling and loss of line of response (LOR) and the usual sinogram-based reconstruction method is not applicable. Therefore, the maximum likelihood-expectation maximization (MLEM) method (Shepp and Vardi 1982) was used in the LOR-based reconstruction using Siddon's algorithm (Siddon 1985).

In this study, only the detector sensitivity correction was applied while ignoring the other possible correction factors to account for scattering or absorption.

2.3. Phantom configuration

Two custom-made phantoms were used in our measurements. The first phantom was a polycarbonate cylindrical phantom with a width of 20 cm and a diameter of 18 cm. We refer to this phantom as the *cylindrical phantom*. It contained 13 cylindrical radiation sources (each with a diameter of 2 mm and width of 2 mm) that were arranged as shown in figure 2. The other phantom was a polycarbonate plate containing five cylindrical radiation sources of various diameters (i.e. 8, 12, 16, 24, 32 mm) with 1.5 cm width, representing different tumor sizes as shown in figure 3(a). This was attached to an acrylic slab (height: 20 cm, width: 18.5 cm, depth: 0.3 cm) as shown in figure 3(b). In this paper, we refer to this phantom setup as the *tumor phantom*. The radiation sources in both the cylindrical phantom and the tumor phantom used ^{18}F that was homogeneously mixed in a gelatinous medium.

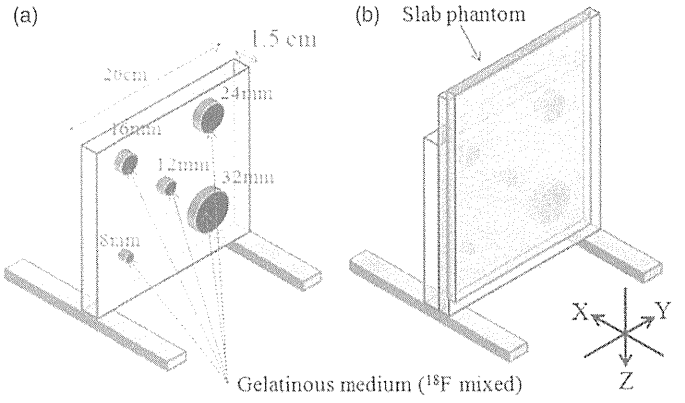

Figure 3. (a) Polycarbonate plate containing ^{18}F-sources of various diameters representing different tumor sizes. (b) The plate in (a) attached to an acrylic slab phantom.

2.4. FWHM of the profile of 2 mm diameter sources

The unique detector geometry of the BOLPs does not allow the use of the filtered back projection reconstruction as specified in the National Electrical Manufactures Association (NEMA) standard which is used for the evaluation of PET detectors. Therefore we used a modified method for image reconstruction based on PEM (Smith *et al* 2004, MacDonald *et al* 2009), which has a detector geometry similar to the BOLPs. PEM devices and the BOLPs have anisotropic spatial resolutions because the detectors do not encircle the object and do not rotate to acquire the full 360° angular sampling required for full three-dimensional tomography. Parallax error caused by the thickness of scintillation crystals is considered (Hoffman *et al* 1989, Lerche *et al* 2005).

We evaluated the FWHM of the profile of 13 cylindrical sources with a diameter of 2 mm and width of 2 mm using the cylindrical phantom shown in figure 2. The ^{18}F activity was 40 kBq ml^{-1}. The projection data were measured for 15 min at a gantry angle of 0°. The image reconstruction via the MLEM method was applied with the pixel size and slice thickness of 1.00 mm and a reconstruction volume of 15 × 15 × 15 cm^3.

2.5. Registration experiments

2.5.1. PDRI registration. PDRI registration was performed by comparing the in-plane digitally reconstructed planar image from the BOLPs and the image obtained from a conventional PET (Discovery ST, General Electric, Schenectady, New York). The pixel size and slice thickness were 3.91 and 3.27 mm, respectively. We placed the tumor phantom in a conventional PET such that the polycarbonate plate was parallel to the longitudinal axis and the center of the plate aligned with the isocenter. Data collection was performed for 15 min.

The tumor phantom was then placed at the isocenter of the BOLPs to obtain the data for the PDRI. Data were also collected for two additional conditions where the tumor phantom was displaced by 2 and 7 mm along the *Y*-axis, away from the isocenter to avoid the observer's bias from trial learning. Each measurement with the BOLPs was carried out for 5 min. The activity of ^{18}F was 20 kBq ml^{-1} and the background activity was 4 kBq ml^{-1}. The gantry angle was fixed at 0°. MLEM image reconstruction was applied with the pixel size and slice thickness of 1.00 mm and a reconstruction volume of 15 × 15 × 5 cm^3. PDRIs corresponding

to 1, 3 and 5 min measurements were generated for each setup position. Image registration based on the PDRI for each setup position was performed by five observers. The reference image was reconstructed from a conventional PET image.

2.5.2. Radiographic registration. To compare the accuracy of radiographic and PDRI registrations, we also performed image registration using images obtained from an x-ray CT and a fluoroscopic system. The tumor phantom was placed at the isocenter of the x-ray CT following the same setup as used in the PET measurement. The pixel size and slice thickness were 0.98 and 1.25 mm, respectively. Fluoroscope images of the tumor phantom were also taken using the installed fluoroscopic system in the proton irradiation system. The position of the tumor phantom was subsequently moved along the *Y*-axis to take additional data at 2 and 7 mm from the isocenter. The reference image used in the radiographic registration was the DRR reconstructed from x-ray CT.

2.5.3. Registration accuracy evaluation. To evaluate the accuracy of the registration methods, image registration trials using in-house software were performed for ten trials. Each trial consisted of five different images shown twice to the observers. Five observers estimated the shifts in each trial. From the image registration data, we calculated the registration error (RE) using equation (1). Actual shift (Y_{actual}) was 0, 2 and 7 mm along the *Y*-axis. Z_{obs} and Y_{obs} in the equation refer to the observed translation along the *Z*-axis and *Y*-axis respectively performed by the five subjects. Statistical analysis was performed based on the registration error for both the radiographic and PDRI registrations:

$$\text{RE(mm)} = \sqrt{(Z_{\text{obs}})^2 + (Y_{\text{obs}} - Y_{\text{actual}})^2}. \tag{1}$$

Here RE denotes the registration error, Z_{obs} the observed translation along the *Z*-axis, Y_{obs} the observed translation along the *Y*-axis and Y_{actual} the actual setup couch translation along the *Y*-axis (0, 2, 7 mm).

2.5.4. Statistical analysis. Statistical analysis of our data was performed using JMP 8 (SAS Institute Inc.) software. The mean registration error and standard deviation (SD) for the various diameters were determined based on the acquisition time for data collection (i.e. 1, 3 and 5 min) and modality (BOLPs, x-ray fluoroscopy). Data were analyzed by one-way ANOVA, while the differences among means were analyzed by two-sided Student's *t*-test with the level of statistical significance set to $p < 0.05$.

3. Results

3.1. FWHM of the profile of 2 mm diameter sources

Figure 4 shows the reconstructed in-plane and cross-plane images of the cylindrical phantom corresponding to a gantry angle of 0°. The reconstructed source diameter at the central position was larger than the others due to blurring caused by adjacent sources. The FWHM of each radiation source is shown in figure 5. The mean ± SD for FWHM was 1.8 ± 0.3 mm in the in-plane image and 8.1 ± 1.2 mm in the cross-plane image at a gantry angle of 0°.

3.2. Registration accuracy evaluation

Shown in figure 6 are the PDRIs of the tumor phantom at a gantry angle of 0°. Images from left to right correspond to the three acquisition times (1, 3 and 5 min) for data collection,

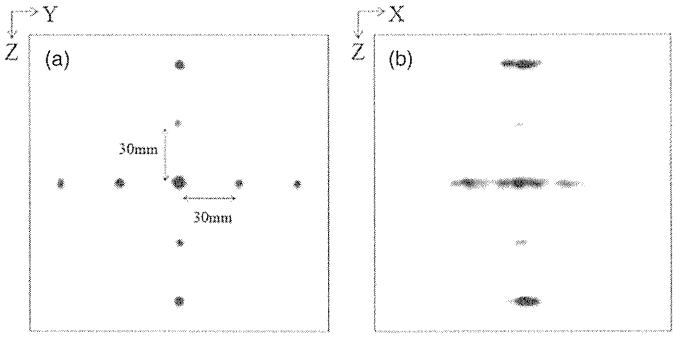

Figure 4. Planar images of the ^{18}F-sources along the (a) in-plane and (b) cross-plane directions reconstructed from the BOLPs data at a gantry angle of 0°.

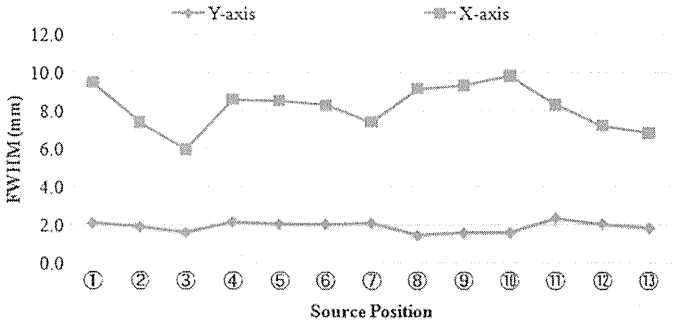

Figure 5. FWHM of the profile of the 2 mm diameter sources in the cylindrical phantom of figure 2.

while those from top to bottom correspond to the positions of the phantom (0, 2 and 7 mm) during data acquisition. The gray-scale window level of the images was adjusted to enhance the contrast. The measured activity at the source increased linearly as a function of acquisition time, and contrast to the background was constant and no inconsistency was observed among the three positions.

Figure 7 shows the variations in the observed PDRI and radiographic registration errors with respect to the acquisition time, phantom position and source diameter. PDRI registration errors were obtained from the registration of the reconstructed PET and BOLPs planar images. The radiographic registration errors were obtained from registration of DRR and portal (x-ray) images. The dependence of the registration error on the phantom position was not seen for each diameter.

Shown in table 1 are the mean ± SD of the registration errors based on our ANOVA. For the diameter of 8 mm the mean registration error of the PDRI registration appears to be influenced by the acquisition time with the longest acquisition time having the least mean registration error. The registration error for the radiographic registration was comparable to that of the shortest acquisition time of 1 min for the PDRI. The differences in the registration error between the image registration modalities listed in table 1 for the 8 mm diameter were found to be significant at a p-value of <0.0001. On the other hand, the mean registration error in all four registration methods for the diameter of 12 mm was found to be statistically insignificant ($p = 0.3545$) with their mean registration error ranging between 0.49 and 0.63. For diameters of 16 and 24 mm, the three acquisition times using the PDRI resulted in similar

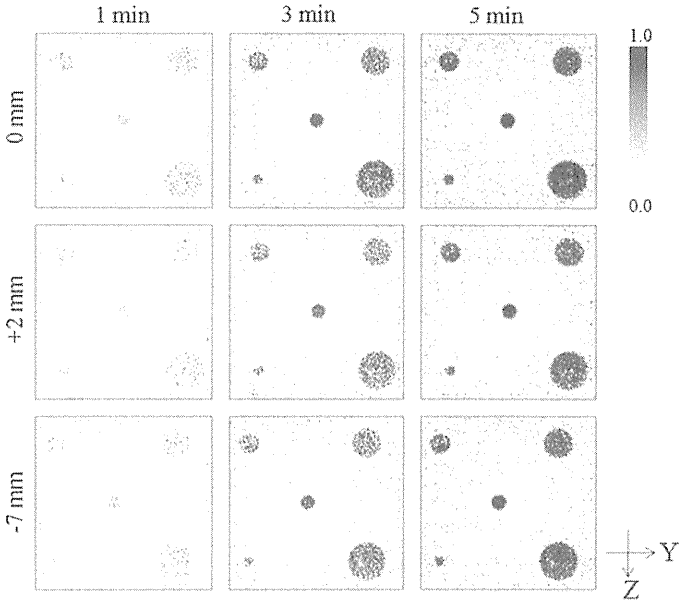

Figure 6. Planar image reconstructions of the ^{18}F-sources in the tumor phantom of figure 3(b). Shown are the results for three phantom positions relative to the isocenter and at the acquisition times of 1 , 3 and 5 min, respectively.

Table 1. Statistical comparison of registration errors from PDRI and radiographic registrations using ANOVA. PDRI registration was performed using reconstructed planar images from PET data (at the acquisition time of 15 min) and BOLPs data (at the acquisition times of 1, 3 and 5 min). Radiographic registration was performed using DRR and portal (x-ray) images.

	Diameter				
Registration method	8 mm	12 mm	16 mm	25 mm	32 mm
PDRI (1 min)	1.07 ± 0.42	0.49 ± 0.34	1.02 ± 0.44	1.28 ± 0.35	1.12 ± 0.39
PDRI (3 min)	0.87 ± 0.29	0.59 ± 0.24	1.01 ± 0.38	1.25 ± 0.29	0.86 ± 0.37
PDRI (5 min)	0.56 ± 0.26	0.60 ± 0.24	1.00 ± 0.34	1.30 ± 0.26	0.88 ± 0.32
Radiographic (x-ray)	0.98 ± 0.28	0.63 ± 0.30	0.87 ± 0.31	0.95 ± 0.20	1.17 ± 0.26
p-value	$<0.0001^*$	0.3545	0.522	0.0003^*	0.0044^*

*Significant ($p < 0.05$).

registration errors and a relatively smaller registration error for the radiographic registration. However, the difference between the PDRI and radiographic registrations was found to be statistically significant only for 24 mm at $p = 0.0003$. A significant difference between the PDRI and radiographic registration errors was obtained for the 32 mm diameter.

The statistical comparisons of the mean registration error and SD for each source diameter obtained from the PDRI registration at 1, 3, and 5 min and the radiographic registration are shown in figures 8 and 9.

For the diameter of 8 mm, the differences in the registration error for the three acquisition times used in the PDRI registration were found to be statistically significant. However, when compared to the registration error of the radiographic registration, only the 5 min PDRI data yielded a significant difference. The mean registration errors for the image registration

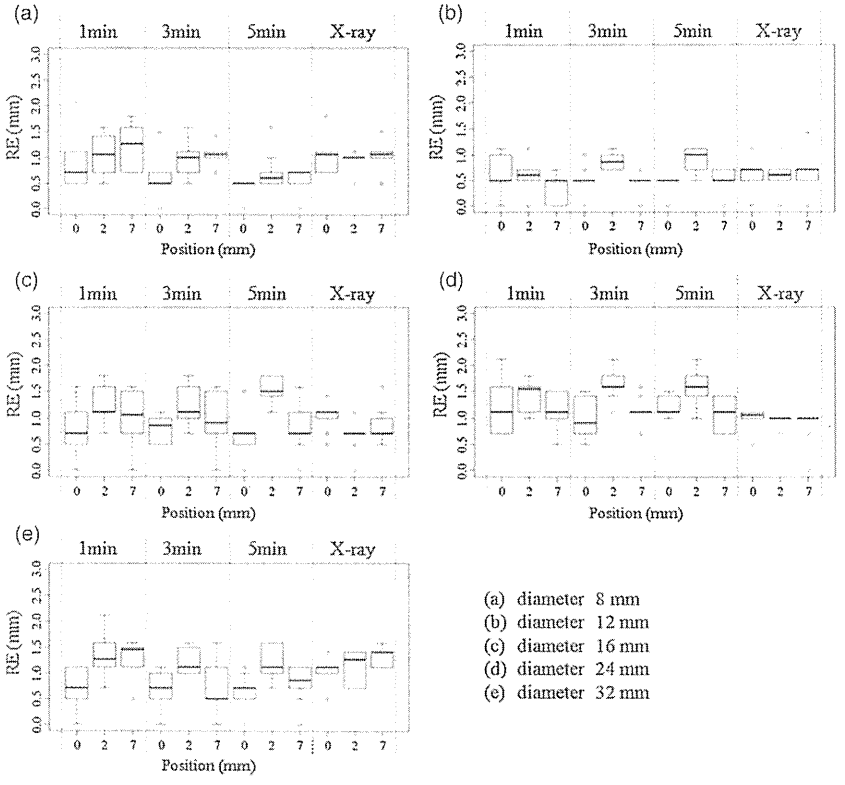

Figure 7. Registration errors for the tumor phantom of figure 3(b). Shown are the results for three phantom positions relative to the isocenter (0), isocenter + 2 mm (2) and isocenter + 7 mm (7) at the acquisition times of 1 , 3 and 5 min, respectively.

conditions shown in figures 8(b) and (c) for diameters of 12 and 16 mm were not statistically different. However, a larger variation in the computed registration error was observed for 16 mm.

For the diameter of 24 mm, the mean registration error obtained for the radiographic registration was found to be significantly smaller compared to those obtained using the PDRI registration method. Furthermore, the acquisition time did not appear to result in significant differences in the mean registration error for the PDRI registration. Like those of the results for the 8 mm diameter, the mean registration error for the 32 mm diameter decreased with the acquisition time in the PDRI registration.

A comparison of the registration error SDs is shown in figure 9 for the various diameters and data acquisition methods. The SDs for most of the results were not statistically different. The image registration SDs of the PDRI at 3 min acquisition time were statistically the same as those of the radiographic registration.

4. Discussion

An overall evaluation of the accuracy of PDRI registration independent of the source size is necessary. We therefore performed a comparative study of the registration error obtained with PDRI and radiographic registrations for a number of hypothetical source sizes. The cumulative

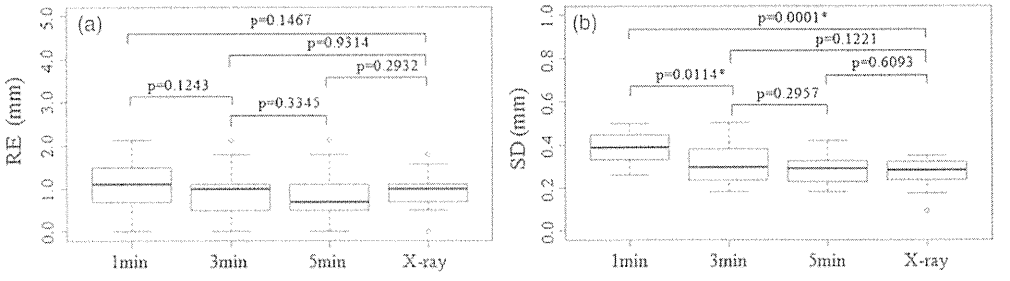

Figure 10. Statistical comparison of (a) the mean registration error and (b) the standard deviation for an overall evaluation using Student's t-test at $p < 0.05$ significance level.

et al (1996) registered 2D portal images with CT data, and their automatic 3D analysis of patient setup accuracy was found to be accurate to within 1 mm in the translational directions. In the clinical evaluation of patient setup errors using portal imaging by Hurkmans *et al* (2001), it was reported that setup errors were less than 2.0 mm (1SD) for head and neck, 2.5 mm (1 SD) for prostate, 3.0 mm (1 SD) for general pelvic and 3.5 mm (1 SD) for lung cancer. The study also noted that the setup verification accuracy varies widely, depending on the treatment site, method of immobilization and institution.

The registration error for the PDRI was lower than that of previously reported radiographic registrations. This could be due to the fact that the image registration was performed with ^{18}F-source itself, not with the skeletal structure, or that there was a phantom dependence. Nevertheless, the registration error for PDRI registration was not significantly different from that of radiographic registration in our experiments. As shown in figure 10(b), the registration error is dependent on the data acquisition time. In order to apply PDRI registration clinically, the acquisition time should be taken into account. A longer acquisition time will result in lower registration error, but it will cause patient discomfort. An optimum acquisition time needs to be considered while maintaining the registration accuracy. However, this is complicated because it depends on the tumor and normal tissue uptake and radiation attenuation in the patient's body. Patient immobilization may also be necessary in order to minimize the effects of inter- and intra-fraction motion caused by patient movement. The effect of respiratory induced motion should be considered in future works.

If FDG is used as the tracer in PDRI registration, it will also be taken up in normal organs such as the brain, liver, kidneys, bladder, etc. This will be a problem in this image registration modality. However, because of the high spatial resolution of our parallel-plane PET system along the in-plane direction, it should be possible to distinguish the tumor FDG uptake from that of the adjacent normal organs which also accumulate FDG. As shown in Figure 4, at the same gantry angle, the corresponding cross-plane image has a much lower resolution and therefore would not be usable for image registration.

Conventional radiographic registration is performed by taking a portal planar image in the LR direction with the gantry at 0° and afterward rotating the gantry to 90° in order to take another portal planar image at the AP direction. These left–right (LR) and anterior–posterior (AP) images are separately registered with corresponding DRR images to complete the radiographic registration process. In our m-IGRT system, the same setup verification procedure using LR and AP images taken separately at different gantry angles will have to be performed. In this case, the PDRI for the LR direction will be the reconstructed in-plane image from the parallel-plane PET data obtained at a gantry angle of 0°. On the other hand, the PDRI for the AP direction will be the reconstructed in-plane image from parallel-plane

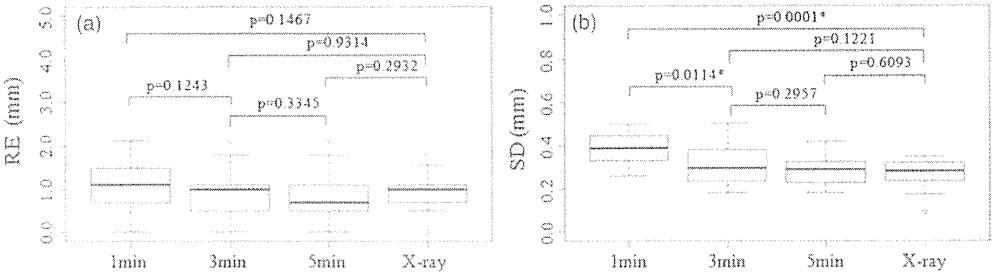

Figure 10. Statistical comparison of (a) the mean registration error and (b) the standard deviation for an overall evaluation using Student's t-test at $p < 0.05$ significance level.

et al (1996) registered 2D portal images with CT data, and their automatic 3D analysis of patient setup accuracy was found to be accurate to within 1 mm in the translational directions. In the clinical evaluation of patient setup errors using portal imaging by Hurkmans *et al* (2001), it was reported that setup errors were less than 2.0 mm (1SD) for head and neck, 2.5 mm (1 SD) for prostate, 3.0 mm (1 SD) for general pelvic and 3.5 mm (1 SD) for lung cancer. The study also noted that the setup verification accuracy varies widely, depending on the treatment site, method of immobilization and institution.

The registration error for the PDRI was lower than that of previously reported radiographic registrations. This could be due to the fact that the image registration was performed with ^{18}F-source itself, not with the skeletal structure, or that there was a phantom dependence. Nevertheless, the registration error for PDRI registration was not significantly different from that of radiographic registration in our experiments. As shown in figure 10(b), the registration error is dependent on the data acquisition time. In order to apply PDRI registration clinically, the acquisition time should be taken into account. A longer acquisition time will result in lower registration error, but it will cause patient discomfort. An optimum acquisition time needs to be considered while maintaining the registration accuracy. However, this is complicated because it depends on the tumor and normal tissue uptake and radiation attenuation in the patient's body. Patient immobilization may also be necessary in order to minimize the effects of inter- and intra-fraction motion caused by patient movement. The effect of respiratory induced motion should be considered in future works.

If FDG is used as the tracer in PDRI registration, it will also be taken up in normal organs such as the brain, liver, kidneys, bladder, etc. This will be a problem in this image registration modality. However, because of the high spatial resolution of our parallel-plane PET system along the in-plane direction, it should be possible to distinguish the tumor FDG uptake from that of the adjacent normal organs which also accumulate FDG. As shown in Figure 4, at the same gantry angle, the corresponding cross-plane image has a much lower resolution and therefore would not be usable for image registration.

Conventional radiographic registration is performed by taking a portal planar image in the LR direction with the gantry at 0° and afterward rotating the gantry to 90° in order to take another portal planar image at the AP direction. These left–right (LR) and anterior–posterior (AP) images are separately registered with corresponding DRR images to complete the radiographic registration process. In our m-IGRT system, the same setup verification procedure using LR and AP images taken separately at different gantry angles will have to be performed. In this case, the PDRI for the LR direction will be the reconstructed in-plane image from the parallel-plane PET data obtained at a gantry angle of 0°. On the other hand, the PDRI for the AP direction will be the reconstructed in-plane image from parallel-plane

PET data obtained at a gantry angle of 90°. The measurement time for each gantry angle is expected to be only a few minutes; therefore, the effects on the acquired parallel-plane PET data of metabolic changes in the body or source activity are negligible.

Additionally, this high spatial resolution will likewise be useful in hypoxic region imaging using FMISO because the hypoxic region distribution in the tumor is complex (Nehmeh *et al* 2008).

5. Conclusion

We performed a basic study to determine the accuracy of image registration using a PET-based molecular image guided method. Planar images were reconstructed from parallel-plane PET data to obtain the PET-based digitally reconstructed planar image (PDRI) used in the registration. In-plane PDRIs had higher resolution and therefore usable for image registration. Phantom experiments using in-plane PDRIs showed that there is no significant difference between radiographic and PDRI registrations. Our results suggest that m-IGRT image registration using PET-based reconstructed planar images along the in-plane direction is feasible for clinical use. Furthermore, the system will provide additional information for image registration when bony structures cannot be recognized with radiographic registration methods.

Acknowledgments

This research was a part of the 'Innovation COE Program for Future Drug Discovery and Medical Care' project and partially supported by the Grant-in-Aid for Special Coordination Funds for Promoting Science and Technology of the Japanese Ministry of Education, Culture, Sports, Science and Technology. The authors are also grateful to the assistance given by the Proton Radiotherapy Department of the National Cancer Center, Kashiwa staff during the experiments with the BOLPs. This research was partially supported by Health and Labour Science Research Grants from the Japanese Government.

References

Dong L and Boyer A L 1995 An image correlation procedure for digitally reconstructed radiographs and electronic portal images *Int. J. Radiat. Oncol. Biol. Phys.* 33 1053–60

Ford E C, Chang J, Mueller K, Sidhu K, Todor D, Mageras G, Yorke E, Ling C C and Amols H 2002 Cone-beam CT with megavoltage beams and an amorphous silicon electronic portal imaging device: potential for verification of radiotherapy of lung cancer *Med. Phys.* 29 2913–24

Gilhuijs K G A, van de Ven P J H and van Herk M 1996 Automatic three-dimensional inspection of patient setup in radiation therapy using portal images, simulator images, and computed tomography data *Med. Phys.* 23 389–99

Groh B A, Siewerdsen J H, Drake D G, Wong J W and Jaffray D A 2002 A performance comparison of flat-panel imager-based MV and kV cone-beam CT *Med. Phys.* 29 967–75

Hoffman E J *et al* 1989 PET system calibrations and corrections for quantitative and spatially accurate images *IEEE Trans. Nucl. Sci.* 36 1108–12

Huesman R H *et al* 2000 List-mode maximum-likelihood reconstruction applied to positron emission mammography (PEM) with irregular sampling *IEEE Trans. Med. Imaging* 19 532–7

Hurkmans C W *et al* 2001 Set-up verification using portal imaging: review of current clinical practice *Radiother. Oncol.* 58 105–20

Jaffray D A, Siewerdsen J H, Wong J W and Martinez A A 2002 Flat-panel cone-beam computed tomography for image-guided radiation therapy *Int. J. Radiat. Oncol. Biol. Phys.* 53 1337–49

Lee N Y and Le Q T 2008 New developments in radiation therapy for head and neck cancer: intensity-modulated radiation therapy and hypoxia targeting *Semin. Oncol.* 35 236–50

Lerche C W *et al* 2005 Depth of γ-ray interaction within continuous crystals from the width of its scintillation light-distribution *IEEE Trans. Nucl. Sci.* 52 560–72

MacDonald L *et al* 2009 Clinical imaging characteristics of the positron emission mammography camera: PEM Flex Solo II *J. Nucl. Med.* 50 1666–75

Munbodh R, Jaffray D A, Moseley D J, Chen Z, Knisely J P S, Cathier P and Duncan J S 2006 Automated 2D–3D registration of a radiograph and a cone beam CT using line-segment enhancement *Med. Phys.* 33 1398–411

Nehmeh S A *et al* 2008 Reproducibility of intratumor distribution of ^{18}F-fluoromisonidazole in head and neck cancer *Int. J. Radiat. Oncol. Biol. Phys.* 70 235–42

Nishio T *et al* 2005 Distributions of β+ decayed nuclei generated in the CH_2 and H_2O targets by the target nuclear fragment reaction using therapeutic MONO and SOBP proton beam *Med. Phys.* 32 1070–82

Nishio T *et al* 2006 Dose-volume delivery guided proton therapy using beam online PET system *Med. Phys.* 33 4190–7

Nishio T *et al* 2010 The development and clinical use of a beam on-line PET system mounted on a rotating gantry port in proton therapy *Int. J. Radiat. Oncol. Biol.Phys.* 76 277–86

Pouliot J *et al* 2005 Low-dose megavoltage cone-beam CT for radiation therapy *Int. J. Radiat. Oncol. Biol. Phys.* 61 552–60

Raylman R R *et al* 2008 The positron emission mammography/tomography breast imaging and biopsy system (PEM/PET): design, construction and phantom-based measurements *Phys. Med. Biol.* 53 637–53

Shepp L A and Vardi Y 1982 Maximum likelihood reconstruction for emission tomography *IEEE Trans. Med. Imaging.* 1 113–22

Siddon R L 1985 Fast calculation of the exact radiological path for a three dimensional CT array *Med. Phys.* 12 252–5

Smith M F *et al* 2003 Analysis of factors affecting positron emission mammography (PEM) image formation *IEEE Trans. Nucl. Sci.* 50 53–9

Smith M F *et al* 2004 Positron emission mammography with tomographic acquisition using dual planar detectors: initial evaluations *Phys. Med. Biol.* 49 2437–52

Som P *et al* 1980 A fluorinated glucose analog, 2-fluoro-2-deoxy-D-glucose (F-18): nontoxic tracer for rapid tumor detection *J. Nucl. Med.* **21** 670–5

Wienhard K *et al* 2002 The ECAT HRRT: performance and first clinical application of the new high resolution research tomograph *IEEE Trans. Nucl. Sci.* 49 104–10

Yamaya T, Hagiwara N, Obi T, Yamaguchi M, Kita K, Ohyama N, Kitamura K, Hasegawa T, Haneishi H and Murayama H 2003 DOI-PET image reconstruction with accurate system modeling that reduces redundancy of the imaging system *IEEE Trans. Nucl. Sci.* 50 1404–9

Zhang J *et al* 2007 Study of the performance of a novel 1 mm resolution dual-panel PET camera design dedicated to breast cancer imaging using Monte Carlo simulation *Med. Phys.* 34 689–702

JJCO Japanese Journal of Clinical Oncology

Jpn J Clin Oncol 2011;41(4)462–468
doi:10.1093/jjco/hyq231
Advance Access Publication 22 December 2010

Long-term Outcomes of Fractionated Stereotactic Radiotherapy for Intracranial Skull Base Benign Meningiomas in Single Institution

Shunsuke Onodera[1,*], Hidefumi Aoyama[1], Norio Katoh[1], Hiroshi Taguchi[1], Kouichi Yasuda[1], Daisuke Yoshida[1], Ken Surtherland[2], Ryusuke Suzuki[2], Masayori Ishikawa[2], Bengua Gerard[2], Shunsuke Terasaka[3] and Hiroki Shirato[2]

[1]Department of Radiation Medicine, Hokkaido University Graduate School of Medicine, [2]Department of Medical Physics, Hokkaido University Graduate School of Medicine and [3]Department of Neurosurgery, Hokkaido University Graduate School of Medicine, Sapporo, Japan

*For reprints and all correspondence: Shunsuke Onodera, Department of Radiation Medicine, Hokkaido University Graduate School of Medicine, North 15, West 7, Kita-ku, Sapporo 060-8638, Japan. E-mail: m950086@jasmine.ocn.ne.jp

Received May 6, 2010; accepted November 21, 2010

Objective: To investigate the outcome of linac-based fractionated stereotactic radiotherapy over the last 10 years for intracranial skull base benign meningiomas in patients who were inoperable, who had residual tumors with some components of high mitotic index after surgery and who experienced relapse of the tumor.

Methods: Twenty-seven patients with intracranial skull base benign meningiomas treated with fractionated stereotactic radiotherapy were retrospectively reviewed. Twenty-seven cases were diagnosed as benign meningiomas on pathological (17 cases) or radiological (10 cases) examination. The median follow-up time was 90 months after initial treatment and 63 months after fractionated stereotactic radiotherapy. The median biological equivalent dose calculated using an α/β ratio of 2.0 Gy was 82.0 Gy (range, 60–106 Gy).

Results: The 5-year overall survival was 95.7 (95% confidence interval: 87.3–100)% after initial treatment and 96.2 (88.8–100)% after fractionated stereotactic radiotherapy. The 5-year overall survival and local control rate of patients who received fractionated stereotactic radiotherapy alone were both 100%. The 5-year progression-free survival and local control rate after fractionated stereotactic radiotherapy were all 100% with a tumor volume of <9.1 cc and 68.2 (37.2–99.2) and 75.8 (45.2–100)% for the tumors 9.1 cc, respectively. The difference was significant in progression-free survival ($P = 0.022$) and local control rate ($P = 0.044$). The local control rate was significantly worse in patients who received fractionated stereotactic radiotherapy for relapsed tumors ($P = 0.01$). No late radiation damage was observed in the follow-up period.

Conclusions: The long-term outcome suggests that fractionated stereotactic radiotherapy is a safe and effective treatment for intracranial skull base benign meningioma, especially for those who have tumors <9.1 cc or would receive fractionated stereotactic radiotherapy with or without surgery as the initial treatment.

Key words: radiation therapy – meningioma – stereotactic – skull base – fractionation

INTRODUCTION

Radiotherapy is increasingly being used for the treatment of meningiomas after incomplete resection, after recurrence and when tumor histology is atypical or malignant (1,2). When meningiomas are located in the intracranial skull base region, tumor excision is frequently incomplete and even biopsy can be hazardous (1). Therefore, it is a matter of

debate whether the use of radiotherapy should be used when the residual tumor is still small as the primary treatment or should be reserved as a potential salvage treatment for the residual tumor enlarged (3).

Stereotactic radiosurgery (SRS) has been proven useful for reducing unnecessary irradiation to the normal tissue surrounding meningiomas and provides an excellent local control rate (LCR) for small to mid-size skull base meningiomas (3,4). Three-dimensional conformal radiotherapy (3D-CRT) and fractionated stereotactic radiotherapy (FSRT) are expected to be useful for further reducing the possibility of late adverse reactions, even for relatively large tumors (5,6). Although there were several precise reports from a few institutions about the long-term outcome after FSRT (5–8), we are still short of knowledge about the treatment results of FSRT with the median follow-up longer than 60 months for intracranial meningioma.

We began using FSRT 15 years ago for patients with intracranial skull base meningiomas, principally for patients who were inoperable, who had residual tumors with some components of high mitotic index or high MIB-1 index, who experienced relapse of the tumor. In this study, we retrospectively reviewed our long-term results for FSRT of intracranial skull base benign meningiomas in order to investigate the usefulness and prognostic factors of this treatment.

PATIENTS AND METHODS

Patients

The outcome of 27 patients with intracranial skull base benign meningiomas treated with FSRT at Hokkaido University Hospital between May 1994 and February 2009 was retrospectively reviewed. Our treatment policy was to apply FSRT principally for those patients with intracranial skull base meningiomas who were inoperable, who had residual tumors or who experienced relapse of the tumor.

The patients' characteristics are summarized in Table 1, which were classified by the treatment category. In our cases, diagnosis was based on pathological examinations in 17 patients and radiological characteristics in 10 patients. The tumor was located at lateral structures in 17 (anterior fossa in 2, middle-lateral sphenoid wing in 8 and cerebellopontine angle and posterior fossa in 7 patients) and at central structures in 10 patients (cavernous sinus and tuberculum sellae in all 10 patients). The median tumor volume was 9.1 (range: 1.1–86.1) cc in all benign meningiomas. The median tumor volume in the initial treatment group was smaller than that in the salvage treatment group (6.3 vs. 12.3 cc), but there was no significant difference statistically ($P = 0.139$; Mann–Whitney test).

In this study, 11 patients were treated with FSRT alone as the initial treatment: 1 after biopsy (Simpson's grade V) and 10 after radiological diagnosis. Radiotherapy was used as a part of the initial treatment after incomplete excision in 4 patients and as a salvage treatment for tumor recurrence after surgery in 12 patients. The number of surgical procedures before FSRT was 1, 2 and 3 in 10, 5 and 1 patients, respectively. Patients who received open biopsy or surgery were classified according to Simpson's grade (9). Simpson's grade II (complete removal and coagulation of dual attachment) and IV (subtotal resection) surgery before radiotherapy was performed in 1 and 15 patients, respectively. Only one patient received biopsy (Simpson's grade V).

Table 1. Patients' characteristics

Factors	Initial treatment group	Salvage treatment group	Total
Total	15	12	27
Diagnosis			
Pathological diagnosis	5	12	17
Radiological diagnosis	10	0	10
Sex			
Male	1	6	7
Female	14	6	20
Age			
Mean (range)	60.3 (18–78)	45.5 (14–72)	53.7 (14–78)
Tumor site			
Lateral	11	6	17
Central	4	6	10
Gross tumor volume			
Median (range) (cc)	6.3 (1.1–58.9)	12.3 (2.5–86.1)	9.1 (1.1–86.1)
Simpson's grade			
I	0	0	0
II	0	1	1
III	0	0	0
IV	4	11	15
V	1	0	1
Radiotherapy alone	10	0	10

Radiation Therapy Method

The gross tumor volume (GTV) was taken as the gross tumor shown on computed tomography (CT) with or without magnetic resonance imaging (MRI). The clinical target volume (CTV) was equal to the GTV, post-operative tumor bed or both in this study. The planning target volume (PTV) was 2–3 mm geometric expansion of the CTV. In delineating GTV, MRI co-registered with CT was used in 18 recent patients, and only the CT information was used for the remaining 9 patients.

Treatment planning systems were Focus or Xio (CMS Japan, Japan). A dose calculation algorithm used for the skull base meningiomas was the Clarkson method or the

convolution method. Stereotactic radiotherapy was carried out by using a 6 or 10 MV linear accelerator (LINAC) (2100C: Varian, Palo Alto, CA, USA; EXL15DP: Mitsubishi, Japan) with an in-house developed LINAC-based SRT system. Three-dimensional non-coplanar, single isocenter and the technique using multileaf collimator (MLC) were used. Three to eight static non-coplanar ports with the conformal fields were used in general. The width of these leafs was 5–10 mm at the isocenter. The dose was prescribed at the isocenter and defined as 100% in the dose distribution profile. MLCs were opened to cover PTV by a 90–95% isodose shell. The maximum dose point was always situated near the isocenter with the dose <110% (Fig. 1).

Patients were fixed by using a thermo-plastic mask and a custom-made head rest system. The dose to the optic chiasm was limited to ≤46 Gy. The total dose was 48–54 Gy in 26 cases and 32 Gy in 1 case using 2.0 Gy as the daily dose. When these radiation schedules were converted into the biological equivalent dose (BED) using an α/β ratio of 2.0 Gy, the median BED dose was 82.0 Gy (range: 52–90 Gy).

Follow-up and Statistical Analyses

The median follow-up time was 90 months (range: 21–209 months) after initial treatment, surgery or FSRT. The median follow-up time was 63 months (range: 19–154 months) after FSRT. More than 70% of patients were followed longer than 36 months after FSRT. Patients were periodically monitored by physical as well as radiographic examination in Hokkaido University Hospital and related hospitals. Local tumor progression (PD) was scored when the maximum diameter of the tumor increased 2 mm or more and partial reaction was scored when the diameter decreased 2 mm or more. The LCR was defined as no change or decrease of the tumor volume in the anatomical region consistent with the PTV of the treatment planning image. When more than 80% of the relapsed tumor volume was outside of the PTV, the recurrence was defined as out of field (10). In-field (>95% of the relapsed tumor volume in the PTV), marginal (20–95% of the relapsed tumor volume in the PTV), and out-of-field (less than 20% of the relapsed tumor volume in the PTV) recurrence were defined in this study.

Statistical analyses were conducted by using commercially available software (SPSS v18; IBM Inc., Chicago, IL). The overall survival (OS) and LCR were calculated from the date of the initiation of radiotherapy using the Kaplan–Meier method, and statistical evaluations were carried out by the log-rank test.

RESULTS

The OS, progression-free survival (PFS) and LCR at 5 years after initial treatment were 95.7 [95% confidence interval (CI): 87.3–100], 91.6 (80.4–100) and 95.5 (86.9–100)%.

The OS, PFS and LCR at 5 years after FSRT were 96.2 (88.8–100), 84.6 (67.7–100) and 88.6 (72.9–100)%.

Partial response was achieved in two benign patients, and the other patients with local control experienced no change of tumor volume. Three (11%) patients experienced in-field recurrence. These tumors had received Simpson's grade IV surgical resection. One patient had progression disease out of irradiation field. The recurrent cases were observed at the posterior fossa (at 55 and 81 months) in two patients, and at the cavernous sinus and tuberculum (at 19 and at 27 months) in two patients. These four recurrent cases are summarized in Table 2. No marginal recurrence was observed.

Univariate analyses were performed on OS, PFS and LCR after FSRT for patients with benign meningioma (Table 3). The female patients had significantly better PFS ($P = 0.009$) and LCR ($P = 0.04$) than the male patients. The 5-year OS, PFS and LCR after FSRT were all 100% for the benign meningiomas with a tumor volume of <9.1 cc and these parameters were 91.7 (76.0–100), 68.2 (37.2–99.2) and 75.8 (45.2–100)% for the tumors >9.1 cc, respectively. The difference was significant in PFS ($P = 0.022$) and LCR ($P = 0.044$) (Fig. 2).

In this study, the 11 patients who received FSRT alone had 100% OS, 88.9% PFS and 100% LCR at 5 years, respectively. The OS, PFS and LCR of patients who received FSRT with or without surgery as the initial treatment ($n = 15$) were 100, 91.7 and 100%, whereas those of patients who received FSRT for relapse ($n = 12$) were 90.9, 68.2 and 68.2%, respectively. The LCR was significantly worse in patients who received FSRT for a relapsed tumor ($P = 0.01$). A higher biological radiation dose, BED, was paradoxically associated with a lower PFS and LCR. The median tumor volume was larger (11.0 vs. 6.7 cc) and the ratio of patients with relapsed tumor was higher (7/11 vs. 5/16) in the higher

Figure 1. Dose distribution of FSRT for an intracranial benign meningioma. FSRT, fractionated stereotactic radiotherapy.

Table 2. The characteristics of patients with skull base benign meningioma who experienced tumor recurrence after FSRT either in-field or out-of-field

No.	Age	Sex	Primary site	Gross tumor volume (cc)	Simpson's grade	FSRT for relapsed tumor	Dose/fraction (Gy/fraction)	Local control	Recurrent site	Relapse (months)	Survival times	Final status
1	78	M	Cavernous sinus	58.9	Grade V	No	54 Gy/27fr	NC	Out-of-field	27	27	Alive
2	35	M	Cerebellopontine angle	9.75	Grade IV	Yes	54 Gy/27fr	PD	In-field	81	81	Alive
3	51	M	Cerebellopontine angle	13.9	Grade IV	Yes	44 Gy/22fr + 10 Gy/4fr	PD	In-field	55	55	Alive
4	58	F	Tuberculum sellae	24.9	Grade IV	Yes	54 Gy/27fr	PD	In-field	19	20	Death

FSRT, fractionated stereotactic radiotherapy; NC, no change; PD, progression of disease.

Table 3. The univariate analysis of prognostic factors after FSRT in patients with skull base benign meningiomas

Factor	5-year OS (95% CI)	*P* value	5-year PFS (95% CI)	*P* value	5-year LCR (95% CI)	*P* value
Age						
>60 ($n = 11$)	100	0.429	87.5 (64.6–100)	0.703	100	0.219
≤60 ($n = 16$)	93.8 (81.8–100)		82.0 (58.1–100)		82.0 (58.1–100)	
Gender						
Female ($n = 20$)	95.0 (85.4–100)	0.584	94.7 (84.7–100)	0.009	94.7 (84.7–100)	0.04
Male ($n = 7$)	100		55.6 (7.0–100)		66.7 (13.4–100)	
Gross tumor volume						
<9.1 cc ($n = 14$)	100	0.28	100	0.022	100	0.044
≥9.1 cc ($n = 13$)	91.7 (76.0–100)		68.2 (37.2–99.2)		75.8 (45.2–100)	
Planning method						
With MRI fusion ($n = 18$)	94.1(82.9–100)	0.467	86.5 (69.1–100)	0.229	93.8 (81.8–100)	0.473
Without MRI fusion ($n = 9$)	100		87.5 (64.6–100)		87.5 (64.6–100)	
Treatment for recurrence						
No ($n = 15$)	100	0.243	91.7 (76.0–100)	0.102	100	0.013
Yes ($n = 12$)	90.9 (73.8–100)		68.2 (27.6–100)		68.2 (27.6–100)	
Biological effective dose (Gy) ($\alpha/\beta = 2$)						
≥85 ($n = 11$)	90.9 (73.8–100)	0.243	60.6 (21.8–99.4)	0.006	68.2 (27.6–100)	0.013
<85 ($n = 16$)	100		100		100	

OS, overall survival; CI, confidence interval; PFS, progression-free survival; LCR, local control rate; MRI, magnetic resonance imaging.

dose group than the lower dose group, although the difference did not reach the level of statistical significance.

No adverse event was observed in the follow-up period. No optical injury, temporal lobe injury or hydrocephalus, or symptoms related to radiotherapy were observed.

DISCUSSION

The median dose used in the present study is 48–54 Gy with daily dose of 2.0 Gy. It is lower than the dose used in the Heiderberg study (5,7), in which the mean radiation dose was 56.8 Gy (±4.4 Gy), and higher than the dose used in the French study (8), in which 45 Gy with daily dose of 1.8 Gy was used. Since a dose–response curve for normal tissues and tumor changes rapidly at the dose range from 40 to 60 Gy with 1.8–2 Gy fractional dose, our results add new biological data for the meningioma and surrounding normal tissue with the long follow-up.

We found that the OS and LCR were 100% at 5 years after FSRT alone for patients with benign skull base meningioma who received FSRT as the initial treatment. This is consistent with a recent article by Korah et al. (6) in which the 8-year LCR was 94% after radiotherapy alone for

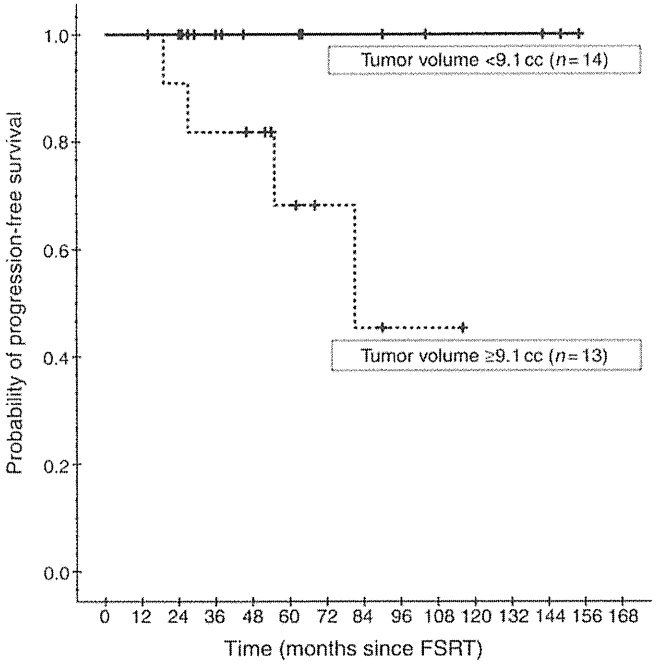

Figure 2. Progression-free survival curves according to the tumor volume. The patients were divided at a median volume of 9.1 cc.

42 patients. Lee et al. (10) also reported a 96.9% LCR at 5 years after SRS alone for 83 patients with cavernous sinus meningiomas. Other series have also suggested a high LCR after radiotherapy alone for benign meningiomas (4,5,11).

After incomplete surgical resection of Simpson's grade III or IV, the recurrence rate of meningiomas is high without radiotherapy (12,13). The recurrence rates for skull base meningioma are especially high, because total resection is much more difficult at this site than at other sites (12,14,15). Adjuvant FSRT immediately after subtotal resection has been suggested to reduce the recurrence rate without lowering the complication rate compared with previous radiotherapy (1,16,17). Previous reports have suggested that radiotherapy for recurrent meningioma is more difficult than radiotherapy used as the initial treatment (14,18). Condra et al. (1)reported that the cause-specific survival was better in patients who received radiotherapy immediately after subtotal resection than those who did not receive radiotherapy. Milker-Zabel et al. (5) also found that patients treated for recurrent meningioma showed a trend toward decreased PFS compared with patients treated with primary therapy, after biopsy or after subtotal resection ($P < 0.06$) in 179 patients with benign or atypical meningiomas.

Our results also suggested that better LCR were obtained for patients who received FSRT with or without surgery as the initial treatment than for those who received FSRT for relapsed tumors. However, the number of patients who were surgically treated and had residual tumor in our institution is uncertain. A small amount of residual benign meningioma after total or subtotal removal often does not enlarge or become symptomatic. Therefore, there is a possible bias that delayed irradiation was given for a poor prognosis group with a tendency of enlargement and irradiation was not required at all for the majority of patients in a good prognosis group. Precise selection criteria for the early irradiation after surgery are warranted to reduce the unnecessary irradiation for the good prognosis group.

The poorer outcome for recurrent meningioma is likely due to the progressive nature of some meningiomas or a mixed component of atypical meningioma (4,19,20). Meningiomas have been reported to obtain radioresistance or a component of malignant transformation as a natural course of the disease (20–23).

Considering that relapsed meningiomas often contain a progressive component, the treatment policy of applying radiotherapy only in the case of relapsed tumors causes a selection bias in the treatment outcome. The progressive nature of some meningiomas may also result in a leading bias with the treatment policy. Our study showed that the 5-year OS was 96.3% after any initial treatment and 88.2% after FSRT for the same patients' group. We summarized the previous studies of SRS and FSRT in Table 4 and found that our results contained the largest proportion of the relapsed tumors in these series. The tendency for the outcome to be better in the series with a lower proportion of relapsed tumors was not negligible. The lack of these biases may partly explain the excellent results in the group that received radiotherapy alone. The present study suggested that the selection bias and leading bias must be held in mind when we compare the treatment results of radiotherapy among different institutions or compare it with surgical series.

This study showed that the tumor volume was a significant prognostic factor as reported previously (5,22). We summarized the previous studies of SRS and FSRT which discriminated the tumor volume of benign tumors from atypical and malignant meningiomas (Table 4). The median tumor volume was 10 cc less in the majority of studies (4,10,11,24–29). The 5-year PFS and LCR values were more than 90% in these series. This study showed that our results of FSRT for tumors <9.1 cc (median) were as good as those in the previous studies. However, for the total patient group, including patients with larger tumors, the 5-year PFD and LCR were 84.6 and 88.6%, respectively. This finding is consistent with the results of Subach et al., who reported a mean tumor volume of 13.7 cc and a reduction of 5-year LCR to 86% (24).

Conventional 3D-CRT was reported to achieve excellent results in 1980s–early 1990s when CT and MRI images had 5 mm slice thickness and very precise fixation did not make sense. However, in the late 1990s, treatment planning using images with 1–2 mm thickness began to require precise fixation of the skull. Although there is no randomized studies to compare 3D-CRT and FSRT, FSRT can reduce the dose to the critical part of brain tissue with higher certainty than conventional 3D-CRT in the era of 1–2 mm slice thickness of the medical images. There are two recent reviews comparing different radiotherapy techniques such as 3D-CRT, SRS

Table 4. Previous studies of stereotactic radiosurgery and fractionated stereotactic radiotherapy for skull base benign meningioma in which the median or mean tumor volume was described for benign tumors

Institution	SRS or FSRT	No. of patients	Tumor volume median (range) (cc)	Recurrent cases (%)	Follow-up period median (range) (months)	PFS	LCR
Mayo Clinic (30)	SRS	88	10 (2.3–30)	>3 (3%)	35 (12–83)	95.0%	—
University of Pittsburgh (24)	SRS	60	13.7[a] (0.8–56.8)	>13 (21%)	35[a] (12–101)	—	86.7%
University of Pittsburgh (10)	SRS	155	6.5 (0.5–52.4)	Unknown	39[a] (2–145)	—	93.1%
University Hospital, Verona (25)	SRS	111	8.1[a] (1–20)	0 (0%)	48.2 (12.1–82.5)	96.0%	97.0%
CHU La Timone (4)	SRS	32	2.28[a] (0.25–60)	2 (6%)	56[a] (24–118)	100.0%	—
University of Pittsburgh (26)	SRS	219	5.0 (0.47–56.5)	0 (0%)	29 (2–164)	—	93%
Medical University Graz (28)	SRS	200	6.5 (0.38–89.8)	Unknown	94.8 (60–144)	98.5%	—
Seoul National University (11)	SRS	63	6.3[a] (0.5–18.4)	1 (2%)	77[a] (48–112)	90.2%	—
University of Pittsburgh (29)	SRS	168	6.1 (0.3–32.5)	35 (21%)	72 (–254)	91.0%	97% (at 10 years)
University of California (27)	FSRT	45	14.5 (1.4–65.66)	8 (31%)	36 (12–53)	97.4% (3 years)	—
Hokkaido University (9.1 cc>)	FSRT	14	4.7 (1.1–9.0)	4 (28.6%)	79.0 (27–154)	100.0%	100.0%
Hokkaido University (all cases)	FSRT	27	9.1 (1.1–86.1)	12 (44.4%)	63.0 (19–154)	84.6%	88.6%

SRS, stereotactic radiosurgery.
[a]Mean.

and FSRT (30,31). Elia et al. (30) summarized that FSRT has toxicity equivalent to that of SRS, despite its biased use for larger meningiomas with more complicated volumes. Minniti et al. (31) recommended SRS only for tumors <3 cm away more than 3 mm from the optic pathway because of the high risk of long-term neurological deficits.

Selch et al. (27) reported an encouraging 3-year PFS of 97% after FSRT for patients with a median tumor volume of 14.5 cc using a dose fractionation schedule similar to that in our study. Milker-Zabel et al. (5) have published results of FSRT for 179 skull base meningiomas, achieving 90.5 and 89% recurrence-free survival rates for benign meningiomas and atypical meningiomas, respectively, and using a median dose of 57.6 Gy (range: 45–68 Gy). Their results were excellent considering that the median target volume was as large as 33.6 cm^3 (1–412.6 cm^3) and as many as 141 (44.5%) cases of recurrent disease were included. Eight (4.4%) patients developed new clinical symptoms, such as reduced vision, trigeminal neuralgia and intermittent tinnitus located at the side of the irradiated meningioma after FSRT in their series. The slightly higher dose used in their study might have been the reason for the better tumor control with a little higher complication rate compared with our study. Korah et al. (6) used FSRT, 3D-CRT and SRS for 9, 11 and 22 patients, respectively, and among these, only 1 patient treated with SRS developed a symptomatic radiation-related neurological complication. There were no late adverse reactions in our series (27). Considering that a lower complication rate is an extremely important issue for patients with benign tumors, FSRT is one of the initial treatment options for patients with intracranial skull base meningioma which locate very close to the critical portion of normal brain tissues.

However, in our relapse cases, the LCR was low. We consider that the 2–3 mm PTV margin was sufficient with our FSRT technique by adding MLC margin to cover the PTV with 90–95% isodose line. However, it is not deniable that the high relapse rate of the larger tumors may also be explained by the small PTV margins used in our study. Goldsmith et al. (32) reported that the PFS rate in the group treated with a minimum tumor dose of >52 Gy was better than the group treated with ≤52 Gy (93 vs. 65%; $P = 0.04$). When FSRT was used for treating the case of the tumor located near the organ at risk (OAR), we must have reduced the margin for PTV to exclude the OAR from the high-dose area. Thus, the dose concentration for the tumor was gotten worse than an ideal dose distribution. Intensity-modulated radiotherapy (IMRT) is expected to increase the therapeutic ratio by reducing the dose to normal tissue because IMRT can deliver the prescription dose to the targets without worsen the dose concentration. For improvement of the LCR of those relapse cases, IMRT with a fractionated schedule will be more appropriate than simple FSRT to increase the dose for these tumors without increasing the dose to the surrounding normal tissue (33–36). However, higher radiation dose to the rest of the body and higher cost to the patient must be taken into account for each patient to use IMRT.

In conclusion, the long-term outcome suggests that FSRT is a safe and effective treatment for intracranial skull base benign meningioma, especially for those who have tumors <9.1 cc or would receive FSRT with or without surgery as the initial treatment.

Funding

This study was partly supported by Grant-in-Aid for Scientific Research (no. 21249065) from Ministry of Education, Culture, Sports, Science and Technology, Japan, and a part of this study was presented in the poster session of 51th Annual Meeting of ASTRO in Chicago (USA), 1–5 November 2009.

Conflict of interest statement

None declared.

References

1. Condra KS, Buatti JM, Mendenhall WM, Friedman WA, Marcus RB, Jr, Rhoton AL. Benign meningiomas: primary treatment selection affects survival. *Int J Radiat Oncol Biol Phys* 1997;39:427–36.
2. Whittle IR, Smith C, Navoo P, Collie D. Meningiomas. *Lancet* 2004;363:1535–43.
3. Kondziolka D, Flickinger JC, Perez B. Judicious resection and/or radiosurgery for parasagittal meningiomas: outcomes from a multicenter review. Gamma Knife Meningioma Study Group. *Neurosurgery* 1998;43:405–13; discussion 13–4.
4. Roche PH, Pellet W, Fuentes S, Thomassin JM, Regis J. Gamma knife radiosurgical management of petroclival meningiomas results and indications. *Acta Neurochir (Wien)* 2003;145:883–8; discussion 8.
5. Milker-Zabel S, Zabel A, Schulz-Ertner D, Schlegel W, Wannenmacher M, Debus J. Fractionated stereotactic radiotherapy in patients with benign or atypical intracranial meningioma: long-term experience and prognostic factors. *Int J Radiat Oncol Biol Phys* 2005;61:809–16.
6. Korah MP, Nowlan AW, Johnstone PA, Crocker IR. Radiation therapy alone for imaging-defined meningiomas. *Int J Radiat Oncol Biol Phys* 2010;76:181–6.
7. Milker-Zabel S, Zabel-du Bois A, Huber P, Schlegel W, Debus J. Fractionated stereotactic radiation therapy in the management of benign cavernous sinus meningiomas : long-term experience and review of the literature. *Strahlenther Onkol* 2006;182:635–40.
8. Litre CF, Colin P, Noudel R, Peruzzi P, Bazin A, Sherpereel B, et al. Fractionated stereotactic radiotherapy treatment of cavernous sinus meningiomas: a study of 100 cases. *Int J Radiat Oncol Biol Phys* 2009;74:1012–7.
9. Simpson D. The recurrence of intracranial meningiomas after surgical treatment. *J Neurol Neurosurg Psychiatry* 1957;20:22–39.
10. Lee JY, Niranjan A, McInerney J, Kondziolka D, Flickinger JC, Lunsford LD. Stereotactic radiosurgery providing long-term tumor control of cavernous sinus meningiomas. *J Neurosurg* 2002;97:65–72.
11. Han JH, Kim DG, Chung HT, Park CK, Paek SH, Kim CY, et al. Gamma knife radiosurgery for skull base meningiomas: long-term radiologic and clinical outcome. *Int J Radiat Oncol Biol Phys* 2008;72:1324–32.
12. De Jesus O, Sekhar LN, Parikh HK, Wright DC, Wagner DP. Long-term follow-up of patients with meningiomas involving the cavernous sinus: recurrence, progression, and quality of life. *Neurosurgery* 1996;39:915–9; discussion 9–20.
13. Mathiesen T, Lindquist C, Kihlstrom L, Karlsson B. Recurrence of cranial base meningiomas. *Neurosurgery* 1996;39:2–7; discussion 8–9.
14. Maroon JC, Kennerdell JS, Vidovich DV, Abla A, Sternau L. Recurrent spheno-orbital meningioma. *J Neurosurg* 1994;80:202–8.
15. Black PM, Villavicencio AT, Rhouddou C, Loeffler JS. Aggressive surgery and focal radiation in the management of meningiomas of the skull base: preservation of function with maintenance of local control. *Acta Neurochir (Wien)* 2001;143:555–62.
16. Debus J, Wuendrich M, Pirzkall A, Hoess A, Schlegel W, Zuna I, et al. High efficacy of fractionated stereotactic radiotherapy of large base-of-skull meningiomas: long-term results. *J Clin Oncol* 2001;19:3547–53.
17. Mendenhall WM, Morris CG, Amdur RJ, Foote KD, Friedman WA. Radiotherapy alone or after subtotal resection for benign skull base meningiomas. *Cancer* 2003;98:1473–82.
18. Al-Mefty O, Kadri P, Pravdenkova S, Sawyer JR, Stangeby C, Husain M. Malignant progression in meningioma: documentation of a series and analysis of cytogenetic findings. *J Neurosurg* 2004;101:210–8.
19. Aghi MK, Carter BS, Cosgrove GR, Ojemann RG, Amin-Hanjani S, Martuza RL, et al. Long-term recurrence rates of atypical meningiomas after gross total resection with or without postoperative adjuvant radiation. *Neurosurgery* 2009;64:56–60.
20. Ohba S, Yoshida K, Hirose Y, Ikeda E, Kawase T. Early malignant transformation of a petroclival meningothelial meningioma. *Neurosurg Rev* 2009;32:495–9.
21. Colvett KT, Hsu DW, Su M, Lingood RM, Pardo FS. High PCNA index in meningiomas resistant to radiation therapy. *Int J Radiat Oncol Biol Phys* 1997;38:463–8.
22. Maillo A, Orfao A, Espinosa AB, Sayagues JM, Merino M, Sousa P, et al. Early recurrences in histologically benign/grade I meningiomas are associated with large tumors and coexistence of monosomy 14 and del(1p36) in the ancestral tumor cell clone. *Neuro Oncol* 2007;9:438–46.
23. Nakane Y, Natsume A, Wakabayashi T, Oi S, Ito M, Inao S, et al. Malignant transformation-related genes in meningiomas: allelic loss on 1p36 and methylation status of p73 and RASSF1A. *J Neurosurg* 2007;107:398–404.
24. Subach BR, Lunsford LD, Kondziolka D, Maitz AH, Flickinger JC. Management of petroclival meningiomas by stereotactic radiosurgery. *Neurosurgery* 1998;42:437–43; discussion 43–5.
25. Nicolato A, Foroni R, Alessandrini F, Maluta S, Bricolo A, Gerosa M. The role of Gamma Knife radiosurgery in the management of cavernous sinus meningiomas. *Int J Radiat Oncol Biol Phys* 2002;53:992–1000.
26. Flickinger JC, Kondziolka D, Maitz AH, Lunsford LD. Gamma knife radiosurgery of imaging-diagnosed intracranial meningioma. *Int J Radiat Oncol Biol Phys* 2003;56:801–6.
27. Selch MT, Ahn E, Laskari A, Lee SP, Agazaryan N, Solberg TD, et al. Stereotactic radiotherapy for treatment of cavernous sinus meningiomas. *Int J Radiat Oncol Biol Phys* 2004;59:101–11.
28. Kreil W, Luggin J, Fuchs I, Weigl V, Eustacchio S, Papaefthymiou G. Long term experience of gamma knife radiosurgery for benign skull base meningiomas. *J Neurol Neurosurg Psychiatry* 2005;76:1425–30.
29. Flannery TJ, Kano H, Lunsford LD, Sirin S, Tormenti M, Niranjan A, et al. Long-term control of petroclival meningiomas through radiosurgery. *J Neurosurg* 2010;112:957–64.
30. Elia AEH, Shih HA, Loeffler JS. Stereotactic radiation treatment for benign meningiomas. *Neurosurg Focus* 2007;23:E5.
31. Minniti G, Amichetti M, Enrici RM. Radiotherapy and radiosurgery for benign skull base meningiomas. *Radiat Oncol* 2009;4:42.
32. Goldsmith BJ, Wara WM, Wilson CB, Larson DA. Postoperative irradiation for subtotally resected meningiomas. A retrospective analysis of 140 patients treated from 1967 to 1990. *J Neurosurg* 1994;80:195–201.
33. Khoo VS, Oldham M, Adams EJ, Bedford JL, Webb S, Brada M. Comparison of intensity-modulated tomotherapy with stereotactically guided conformal radiotherapy for brain tumors. *Int J Radiat Oncol Biol Phys* 1999;45:415–25.
34. Pirzkall A, Carol M, Lohr F, Hoss A, Wannenmacher M, Debus J. Comparison of intensity-modulated radiotherapy with conventional conformal radiotherapy for complex-shaped tumors. *Int J Radiat Oncol Biol Phys* 2000;48:1371–80.
35. Pirzkall A, Debus J, Haering P, Rhein B, Grosser KH, Hoss A, et al. Intensity modulated radiotherapy (IMRT) for recurrent, residual, or untreated skull-base meningiomas: preliminary clinical experience. *Int J Radiat Oncol Biol Phys* 2003;55:362–72.
36. Milker-Zabel S, Zabel-du Bois A, Huber P, Schlegel W, Debus J. Intensity-modulated radiotherapy for complex-shaped meningioma of the skull base: long-term experience of a single institution. *Int J Radiat Oncol Biol Phys* 2007;68:858–63.